ELSEVIER

Applied Surface Science 186 (2002) 573–577

applied surface science

www.elsevier.com/locate/apsusc

Emission spectroscopy of carbon-covered iron nanoparticles in different gas atmospheres

K. Elihn*, L. Landström, P. Heszler[1]

The Ångström Laboratory, Department of Materials Chemistry, Uppsala University, Box 538, 751 21 Uppsala, Sweden

Abstract

Black body-like radiation was observed when irradiating ferrocene vapor ($Fe(C_5H_5)_2$) in xenon, argon, helium or hydrogen atmosphere by an ArF excimer laser. The emission originated from carbon-covered iron nanoparticles excited by the laser pulses. Time-resolved spectroscopy of the thermal radiation was performed at different delay times relative to the exciting laser pulse. Particle temperatures were obtained by fitting the calibrated spectra by the Planck equation, taking the emissivity of nanoparticles into consideration. The cooling rates of the nanoparticles and the lifetime of the thermal radiation were determined in the total pressure region of 0.2–50 mbar for the different gas atmospheres. Based on the measured values, accommodation coefficients and deexcitation cross-sections were obtained. These data characterise the inelastic interaction between the nanoparticles and the surrounding gas atmosphere. The iron phase dependence on the cooling rate was examined by X-ray diffraction of nanoparticle film deposits.

Keywords: Nanoparticle; Ferrocene; Iron; Emission spectroscopy; LCVD

1. Introduction

Nanoparticles are of great interest since their properties are size dependent and nanostructured materials can have superior, e.g. electronic, optical and magnetic characteristics compared to the corresponding bulk material. Iron nanoparticles are studied especially for their interesting magnetic properties. The studies have mainly been concerned with giant magneto-resistance [1], high coercive force and superparamagnetism [2,3] of nanostructured materials. b.c.c. iron (α) is known to be ferromagnetic while f.c.c. iron (γ) is either ferromagnetic or antiferromagnetic depending on the lattice parameter and on the symmetry [4]. Recently it has been shown that carbon-covered iron nanoparticles are formed upon irradiation of ferrocene by a pulsed ArF excimer laser [5]. The surrounding carbon layer has the advantage to act as a protective layer against oxidation and isolates the particles from each other. The laser-assisted technique is advantageous since it allows the ambient gas atmosphere to be close to room temperature while the formed particles are heated up by the subsequent laser pulses and thus high temperature phases of the particles can be formed. The phase transition from b.c.c. to f.c.c. iron occurs at 1184 K. Below 1184 K b.c.c. is the stable iron phase, but when using a fast cooling rate with initial temperatures above 1184 K, it is possible to obtain the metastable f.c.c. iron phase even below the transition temperature. In an argon atmosphere, a mixture of b.c.c. and f.c.c. iron content of the nanoparticles were obtained. Therefore, the question arises

* Corresponding author. Tel.: +46-18-4713-737; fax: +46-18-5135-48.
E-mail address: elihn@kemi.uu.se (K. Elihn).

[1] On leave from the research group on Laser Physics of the Hungarian Academy of Sciences.

0169-4332/02/$ – see front matter
PII: S0169-4332(01)00644-4

weather one can change the ratio between the iron phases by applying different cooling rates of the nanoparticles by using different gas atmospheres in the reactor. In addition, it has been shown that the nanoparticles emit black body-radiation from which it is possible to determine the nanoparticle temperature [5–7]. Thus, time resolved spectroscopy enables determination of the cooling rates of the particles, which may give basic data about the inelastic interaction between the nanoparticles and the surrounding ambient gas atmosphere.

Therefore, the aim in this work was on one hand to try to control the iron phase of the nanoparticles by using different gas atmospheres at different pressures in the reactor, and on the other hand to determine the cooling rates of the particles using time-resolved spectroscopy to get a deeper understanding of the heat transfer process. Xenon, argon, helium and hydrogen were used to imply different rates of cooling. The iron phase of the particles was determined as well as the accommodation coefficients and the inelastic deexcitation cross-sections for the different gas atmospheres. The latter parameters reflect the degree of inelasticity in the collisions between the nanoparticles and the gas ambient.

2. Experimental

The experimental set-up for the synthesis of nanoparticles [8] and optical emission spectroscopic measurements [5] have been described in detail earlier. Briefly, an ArF excimer laser ($\lambda = 193\,\text{nm}$) with a pulse width of 16 ns was used for the photolysis of ferrocene at a repetition rate of 50 Hz. The laser beam was aligned through quartz windows of the particle reactor (cross-section 25 cm^2) and it was focused to $0.1\,\text{cm} \times 1.5\,\text{cm}$ at the ferrocene entrance to give a fluence of about 250 mJ/cm^2. At the position of the optical emission spectroscopic measurement, 7 cm downstream of the ferrocene entrance, the fluence was about 100 mJ/cm^2. Either xenon, argon, helium or hydrogen, was used as carrier gas (80 SCCM) of the ferrocene vapor (sublimation temperature 50 °C) and as purge gas (80 SCCM) of the laser beam entrance quartz window yielding a total flow of 160 SCCM. The total pressure was 0.2–50 mbar, and the reactor temperature was set to 60 °C. The emitted light was observed through a quartz window on top of the reactor and coupled into a quartz optical fibre attached to a Czerny–Turner type grating spectrograph. The electronic detection system consisted of a gateable CCD detector and an optical multichannel analyser. A gate pulse width of 500 ns was used for the time-resolved measurements and spectra were recorded at different times from 0 delay up to 15 μs relative to the laser pulse. The overall exposure time was 1 s. The recorded spectra were corrected by the transfer function of the overall optical and electronic detection system, which was obtained by a calibration procedure using a tungsten-strip calibration lamp. The corrected spectra (see Fig. 1a) were fitted by the Planck equation in order to obtain the particle temperature. The emissivity (ε) of the nanoparticles was taken into consideration as ε which is proportional to λ^{-1}, where λ is the wavelength of the emitted light, as it is expected for nanoparticles [7,9]. X-ray diffraction (XRD) was used to determine the iron phase of the nanoparticles and transmission electron microscopy (TEM) to determine their size.

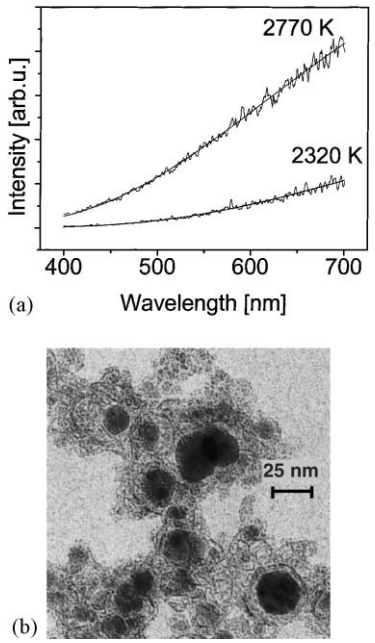

Fig. 1. (a) Calibrated spectra of the observed radiation at two different delay times relative to the laser pulse originating from (b) carbon-covered iron nanoparticles as shown in the TEM micrograph (formed in xenon at 30 mbar). The smooth lines in (a) are the fittings by the Planck equation to the emitted spectra.

3. Results and discussion

Carbon-covered iron nanoparticles, see Fig. 1b, were formed upon laser photolysis of ferrocene in the four different gas atmospheres of xenon, argon, helium and hydrogen. Subsequent laser pulses heated up the nanoparticles and the emitted black body-like radiation, see Fig. 1a, enabled determination of the nanoparticle temperature. The initial particle temperature directly after a laser pulse was approximately the same for all the gas atmospheres at any fixed pressure. Increasing the total pressure reduced the initial particle temperature. The initial particle temperature (500 ns gate pulse and 100 mJ/cm^2 laser fluence) at the lowest total pressure of 0.2 mbar was 2900 ± 50 K. Below 0.2 mbar no black body-like radiation was observed since no particle formation occurred below that pressure [5]. At 50 mbar, the highest pressure used in the experiments, the initial particle temperature was 2600 ± 50 K. Fig. 2a shows the determined particle temperatures at 20 mbar for delay times up to 15 μs after the laser pulse. The initial particle temperature at 20 mbar was 2700 ± 50 K and thereafter the particle temperature decreased. The cooling rate (dT/dt) of the particles is considered linear in the measured temperature range.

The cooling rates of the particles as a function of ambient gas pressure are plotted in Fig. 2b. These were 30–40 K/μs for all the gas atmospheres extrapolated to 0 pressure. This can be related to energy relaxation processes like black body radiation, evaporation and thermionic emission. However, the net effect of dT/dt that is caused by the heat transfer, can be determined from the slopes in Fig. 2b. The cooling rates per unit pressure are listed in Table 1 for the different gas atmospheres. The smallest value was obtained for xenon followed by argon, helium and hydrogen.

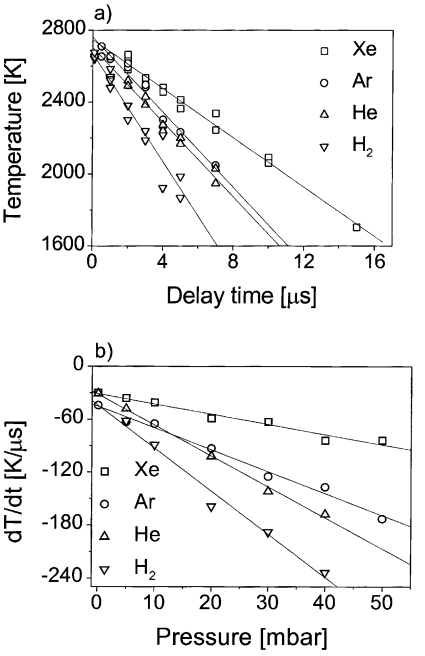

Fig. 2. (a) The nanoparticle temperature versus time after the laser pulse measured at an ambient gas pressure of 20 mbar and (b) the cooling rate of the particles at different total pressures of xenon, argon, helium and hydrogen. The solid lines are linear fittings.

For the cooling rate of the nanoparticles (dT_n/dt), the following expression can be written [10]:

$$\frac{dT_n}{dt} \times C_p = -4\pi r_n^2 \times \zeta f \times \frac{p}{T} \times \left(\frac{k_B T}{8\pi m_{gas}}\right)^{1/2} \times (T_n - T) \quad (1)$$

where C_p is the heat capacity and r_n the radius (see Table 1) of a nanoparticle, respectively, ζ the accommodation coefficient, f the degrees of freedom, p the total gas pressure in the reactor, k_B the Boltzmann constant, m_{gas} the mass of an atom or molecule of the

Table 1
The diameters of the iron core and the total diameter of the nanoparticles including the carbon layer at 30 and 50 mbar of xenon, argon, helium and hydrogen atmosphere and the cooling rate per unit pressure of the nanoparticles

Gas atmosphere	Iron core at 30 mbar (nm)	Total diameter at 30 mbar (nm)	Iron core at 50 mbar (nm)	Total diameter at 50 mbar (nm)	Cooling rate per unit pressure (K/μs mbar)
Xenon	7.4	16.1	6.9	16.2	1.2
Argon	7.0	14.8	6.0	17.6	2.5
Helium	8.8	17.3	9.2	18.8	3.5
Hydrogen	7.9	16.0	8.4	17.0	4.9

ambient gas and T and T_n are the temperature of the reactor gas and the nanoparticles, respectively. Assuming $T \ll T_n$ and constant heat capacity of the particles (although a slight change of the particle size was observed when varying the ambient gas pressure) for the same gas ambient, which are good approximations here, a linear cooling rate versus the ambient pressure is obtained from Eq. (1) in accordance with our results in Fig. 2b. The accommodation factor in Eq. (1) characterises the degree of inelasticity in the collision between the nanoparticles and the ambient gas and it can be determined from the measured parameters. The heat capacity was calculated for the particle diameters shown in Table 1 at the elevated temperatures. Xenon had an accommodation coefficient of 0.18, which means that it removes 18% of the maximum removable energy in each collision. The accommodation coefficient of argon is close to that of xenon and was calculated to be 0.19. For helium and hydrogen ζ was found to be smaller, 0.096 and 0.044, respectively, see Fig. 4.

The phase of the nanoparticles was analysed by XRD. All the deposits made at 30 and 50 mbar showed the presence of both f.c.c. and b.c.c. iron, independent of the particle cooling rate. Even though the particle cooling rate was more than three times faster at 50 mbar for hydrogen compared to xenon, see Fig. 2b, no single phase iron nanoparticle samples were obtained. The mixture of b.c.c. and f.c.c. iron nanoparticles indicates that probably not all particles are heated up to the same high temperature.

The inverse lifetime of the thermal radiation ($1/\tau_{eff}$) of the particles was determined at different pressures of xenon, argon, helium and hydrogen as shown in the Stern–Volmer plots in Fig. 3. This yielded linear

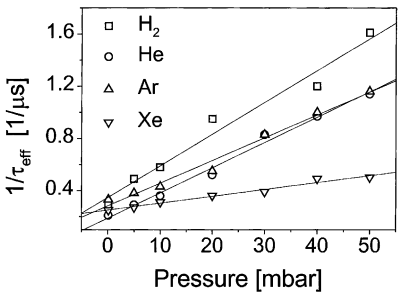

Fig. 3. Stern–Volmer plot showing the quenching of the thermal radiation of the nanoparticles in xenon, argon, helium and hydrogen.

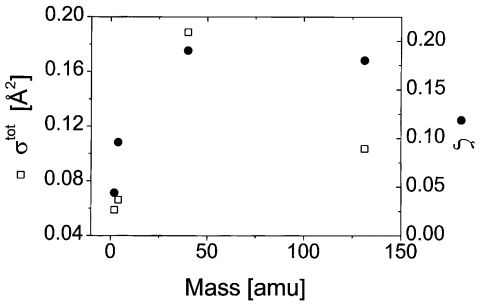

Fig. 4. Deexcitation cross-sections (σ^{tot}) and accommodation coefficients (ζ) versus the mass of hydrogen, helium, argon and xenon.

relations as expected from the Stern–Volmer equation [11]:

$$\frac{1}{\tau_{eff}} = \frac{1}{\tau_{spont}} + \frac{\sqrt{8}}{\pi\mu k_B T} \times \sigma^{tot} \times p \quad (2)$$

where τ_{spont} is the spontaneous lifetime (when no ambient gas is present), μ the reduced mass of the particles and the surrounding gas and σ^{tot} the total deexcitation cross-section of the thermally excited states of the particles. The σ^{tot} values were determined from the plotted slopes in Fig. 3. Hydrogen was the most efficient quencher of the thermal radiation although it had the smallest deexcitation cross-section of 0.059 Å^2, followed by helium (0.066 Å^2), xenon (0.10 Å^2) and argon (0.19 Å^2), see Fig. 4. The reason for this is that the collision number of hydrogen is higher compared to the other gases. The accommodation coefficient and the deexcitation cross-section followed the same trend when plotted versus the mass of the used gases as shown in Fig. 4, except for σ^{tot}(Xe) that was only half the deexcitation cross-section of argon. A heuristic picture can be given to understand these trends. The higher the mass of a gas atom, the "softer" it is (the values of polarisability support this assumption) and, therefore, the degree of inelasticity is higher for the gas atom–nanoparticle interaction.

4. Conclusions

The temperature of carbon-covered iron nanoparticles synthesised by the photolysis of ferrocene could be determined from emitted black body-like radiation. Cooling rates and lifetimes of the thermal radiation of

the particles were determined by using time-resolved spectroscopy. The fastest cooling rate of the particles was obtained in hydrogen, followed by helium, argon and xenon ranging from 4.9 down to 1.2 K/μs mbar. Both b.c.c. and f.c.c. iron was obtained independently on the cooling rates, which reflects that probably not all the particles were heated up above the phase transition temperature. Accommodation coefficients (from 0.044 for hydrogen to 0.18–0.19 for xenon and argon) and deexcitation cross (from 0.059 $Å^2$ for hydrogen to 0.19$Å^2$ for argon) were determined from the measured data and plotted versus the mass of the used gases showing that all but xenon followed the same trend.

Acknowledgements

The Swedish Research Council for Engineering Sciences (TFR) and Göran Gustafssons stiftelse are acknowledged for financial help and Nils Olov Ersson for helping with the XRD.

References

[1] C.B. Peng, S. Zhang, G.Z. Li, D.S. Dai, J. Appl. Phys. 76 (2) (1994) 998.
[2] S. Gangopadhyay, G.C. Hadjipanayis, B. Dale, C.M. Sorensen, K.J. Klabunde, V. Papaefthymiou, A. Kostikas, Phys. Rev. B 45 (17) (1992) 9778.
[3] G.L. Zhang, S.J. Yu, J. Phys.: Condens. Mat. 9 (1997) 1851.
[4] V.L. Moruzzi, P.M. Marcus, J. Kübler, Phys. Rev. B 39 (10) (1989) 6957.
[5] P. Heszler, K. Elihn, M. Boman, J.-O. Carlsson, Appl. Phys. A 70 (2000) 613.
[6] P. Heszler, L. Landström, M. Lindstam, J.-O. Carlsson, J. Appl. Phys. 89 (2001) 3967.
[7] R. Mitzner, E.E.B. Campbell, J. Chem. Phys. 103 (7) (1995) 2445.
[8] K. Elihn, F. Otten, M. Boman, P. Heszler, F.E. Kruis, H. Fissan, J.-O. Carlsson, Appl. Phys. A 72 (2001) 29.
[9] C.F. Bohren, D.R. Huffman, Absorption and Scattering of Light by Small Particles, Wiley, New York, 1983, pp. 83–104.
[10] D. Bäuerle, Laser Processing and Chemistry, 2nd Edition, Springer, Berlin, 1996, pp. 65–68.
[11] W. Demtröder, Laser Spectroscopy, 2nd Edition, Springer, Berlin, 1982, pp. 591–597.